

PAPER

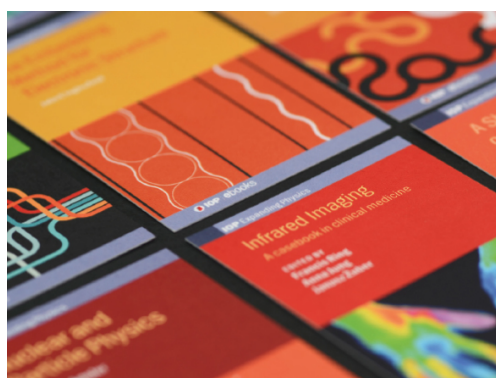
Characterization of the energetics and configurations of hydrogen in vacancy clusters in tungsten

Recent citations

- [A review of surface damage/microstructures and their effects on hydrogen/helium retention in tungsten](#)
Yong-Gang Li *et al*

To cite this article: Qing-Yuan Ren *et al* 2019 *Nucl. Fusion* **59** 106032



View the [article online](#) for updates and enhancements.

**IOP | ebooks™**

Bringing together innovative digital publishing with leading authors from the global scientific community.

Start exploring the collection—download the first chapter of every title for free.

Characterization of the energetics and configurations of hydrogen in vacancy clusters in tungsten

Qing-Yuan Ren^{1,2,a}, Yu-Hao Li^{1,2,a}, Hong-Bo Zhou^{1,2} , Zhong-Zhu Li^{1,2},
L. Cheng^{1,2}  and Guang-Hong Lu^{1,2}

¹ Department of Physics, Beihang University, Beijing 100191, China

² Beijing Key Laboratory of Advanced Nuclear Materials and Physics, Beihang University, Beijing 100191, China

E-mail: hbzhou@buaa.edu.cn (H-B Zhou) and lgh@buaa.edu.cn (G-H Lu)

Received 15 February 2019, revised 20 July 2019

Accepted for publication 29 July 2019


Published 4 September 2019



Abstract

We have explored the retention of hydrogen (H) in tungsten (W) by investigating its dissolution and aggregation in vacancy clusters (VCs) using a first-principles method and thermodynamic models. The solution energy of a single H in the VCs is in the range of -0.99 to -0.64 eV, much lower than that at a mono-vacancy (~ -0.37 eV) and interstitial site (~ 1.01 eV) in W. Such a remarkable discrepancy is rationalized on the electronic interaction of H with its neighboring W atoms, which varies from repulsion to attraction with H moving from perfect crystal to vacancy/VCs. Specifically, the solution/trapping energies of H in VCs can be well categorized by the coordination number of its neighboring W atoms, i.e. the lower the coordination number of W, the stronger the H–W attraction and the lower the H solution/trapping energy. Furthermore, taking the V_9^m cluster as an example, it is observed that the multiple H atoms form a multilayer nested cage configuration at the VC surface initially, and then the stable H_2 molecules form in the center of the VCs. Interestingly, the pre-existing H atoms in the VC inner surface have a shielding effect on the H–W interaction, decreasing the electron density of the central region of the VCs and facilitating the formation of H_2 molecules. Moreover, the desorption temperatures of H in the VCs are also predicted based on the Polanyi–Wigner equation, and are in good agreement with the available thermal desorption spectroscopy experiments. Our calculations provide a good reference to understand the influence of VCs on the retention and evolution of H in W.

Keywords: tungsten, hydrogen, vacancy clusters, energetics and configurations, trapping and retention

 Supplementary material for this article is available [online](#)

(Some figures may appear in colour only in the online journal)

1. Introduction

Due to the good thermal properties and high sputtering threshold energy, tungsten (W) is selected as the primary candidate for plasma-facing materials (PFMs) in ITER [1, 2], the demonstration fusion reactor (DEMO) [3, 4] and other

future fusion reactors. However, the hydrogen (H) isotopes and helium (He) plasma irradiation can significantly deteriorate the structure and properties of W in the fusion environment. The low-energy and high-flux H isotope irradiation causes severe radiation damage, such as surface blistering, erosion and cracking [5]. In addition, the H-induced damage can remarkably enhance the retention of tritium, leading to great concern for the availability and reliability of W-PFM

^aThese authors contributed equally to the work.

under long-term fusion irradiated condition [6]. Hence, the full investigation of H isotopes in W is particularly crucial to fusion operation.

Generally, the thermal equilibrium concentration of H in W is extremely low (about 10^{-15} at.% at room temperature (RT) under 1.3×10^5 Pa of H_2 [7]), owing to its endothermic dissolution process. However, it is found that the retention of H isotopes in W-PFM under H isotope irradiation is much larger than its thermal equilibrium concentration. For example, the deuterium (D) concentration can reach up to ~ 2 at.% at the W near-surface and ~ 0.02 at.% in the bulk at 320 K after D irradiation [8]. This is rationalized by the interaction of H with defects (inherent defects and irradiation-induced defects) in W, such as vacancy, vacancy clusters (VCs), grain boundaries, dislocations, etc [5, 9–14]. Specifically, the thermal desorption spectroscopy (TDS) and transmission electron microscopy experiments suggested that H can be strongly trapped by these defects [15–20]. Generally, there are four different peaks for H desorption temperatures in W (~ 400 , ~ 520 , ~ 640 and ~ 900 K) with the heating rates of $\sim 5 \pm 1.5$ K s^{-1} , corresponding to the de-trapping energy of ~ 0.65 , ~ 1.07 , ~ 1.34 and ~ 2.10 eV, respectively [21, 22]. Vacancy-type defects are the typical defects in materials. VCs and cracks/voids are considered to be the main region for H blistering, substantially promoting the H dissolution and retention in W [16, 17, 23]. In turn, the presence of H can also stabilize the vacancy-type defects in W, and further enhance H retention [24]. Besides, vacancy-type defects are also the common defects of W under high-energy particle irradiation (heavy ions or neutrons) in a fusion environment [24, 25]. More importantly, the VCs induced by pre-irradiation will significantly enhance the H aggregation and retention in W and W alloys [26–29]. Therefore, in order to understand the retention and evolution of H isotopes in W-PFM, the interaction of H with vacancy/VCs should be fully elucidated.

Owing to the extremely small, light and mobile H, the direct observation or measurement for the behavior of H atoms at defects in materials is very difficult [30, 31]. Modelling and simulation become the effective tools to examine the behavior of H and its interaction with defects in materials [32]. First-principles calculations based on density functional theory (DFT) reported that a single H atom prefers to occupy the tetrahedral interstitial site (TIS) in bulk W with the solution energy of ~ 1.00 eV [11, 33–36]. A mono-vacancy can substantially reduce the solution energy of H nearby, owing to the reduction of the electron density [10, 11, 33, 34], and a mono-vacancy can only hold ~ 12 H and ~ 6 H atoms at 0 K and RT [33, 34, 37–39], respectively. Also, the presence of H will in turn facilitate the formation and aggregation of vacancies, leading to the cascading effect [40]. Although the behavior of H–V complexes in W have been investigated in previous studies using the first-principles method, the sizes of the VCs are mainly limited to mono-vacancy and di-vacancy in these works, and thus the behavior of H in VCs remains to be elucidated. Considering the different available volume and the electronic environment, the behavior of H in large VCs is significantly different from that in a mono-/di-vacancy. To address this issue, great effort has been made by employing

large-scale simulations, such as molecular dynamics (MD), kinetic Monte Carlo (KMC), etc, based on the empirical interatomic potential or energetic results from DFT calculations [39, 41–46]. Although these large-scale simulations provide some useful information for the interaction of H with VCs in W, such as the binding energy of large H–V complexes and the temperature-dependent variation of cluster concentrations [39, 42], these results are strongly dependent on the interatomic potential employed [47, 48] and some important characteristics (such as H_2 formation that is proposed by experiments [9, 17]) cannot be reproduced by MD and KMC simulations. Consequently, in order to accurately describe the behavior of H and construct a predictive model for its kinetic evolution, a detailed first-principles calculation for the interaction of H with VCs is essential.

In the present work, the dissolution and aggregation of H in the vacancy/VCs have been systematically investigated by employing the first-principles approach and thermodynamic models. The trapping energies of H in the VCs (-2.00 to -1.65 eV) are much lower than that at a mono-vacancy (-1.38 eV) in W. Specifically, the H solution/trapping energies are well categorized by the coordination number of neighboring W atoms. The lowest H solution/trapping energy in the VCs corresponds to the interaction of H with four-coordination-number W. Interestingly, a distinct multi-layered configuration is observed for multiple H atoms at the inner surface of the VCs, and eventually the H_2 molecules are formed in the center of the VCs. This can be rationalized by the shielding effect of pre-existing H atoms on the H–W interaction, which reduces the electron density of the center of the VCs and facilitates the formation of H_2 molecules. Besides, the predicted desorption temperatures of H in the VCs are in good agreement with available TDS experiments. According to these results, we propose that the VCs are crucial to the retention and evolution of H, which deepens our understanding of the desorption of H isotopes in W.

2. Computational methods

The DFT calculations were conducted in the Vienna *ab initio* simulation package [49, 50]. The projector augmented wave pseudo-potentials developed by Perdew and Wang (PW91) [51] based on the generalized gradient approximation were employed to describe the electronic exchange and correlation part, i.e. six valence electrons for W ($6s^2 5d^4$) and a single 1s valence electron for H. A 250 atom ($5 \times 5 \times 5a_0$) supercell was used in all calculations, and the corresponding Brillouin zone was sampled by Monkhorst–Pack [52] form with k -point mesh density of $3 \times 3 \times 3$. The cut-off energy and the width of the Meshfessel–Paxton smearing was set to be 400 and 0.20 eV, respectively. In the present work, all calculations were performed without spin polarization. Unless otherwise stated, ISIF = 3 was employed in all calculations, corresponding to the fully relaxed edatomic position and the shape and volume of the supercell. The ionic relaxation was continued with the force convergence criterion of 0.01 eV \AA^{-1} for all atoms. Furthermore, the zero-point energy (ZPE)

Table 1. Solution energy (eV) of interstitial H in W. Corresponding electronic contribution (EC), mechanical contribution (MC) and atomic distances (Å) of H with 1 NN and 2 NN W are also presented.

		Fully relaxed		Partly relaxed		Unrelaxed	
		TIS	OIS	TIS	OIS	TIS	OIS
Without ZPE	E^{sol}	0.89/0.88 ^a /0.86 ^b	1.28/1.26 ^{a,b}	0.90	1.29	1.18	1.96
	MC	0.22	0.47	0.22	0.46	—	—
	EC	0.67	0.81	0.68	0.83	1.18	1.96
With ZPE	ZPE	0.26	0.16	0.27	0.16	0.31	0.04
	E^{sol}	1.01/1.00 ^a	1.30	1.03	1.31	1.35	1.86
H–W distance	1 NN	1.85	1.75	1.85	1.75	1.77	1.59
	2 NN	2.88	2.25	2.88	2.25	2.86	2.25

^a Zhou et al [35].^b Heinola et al [57].

corrections were also considered because H is the lightest element. More details for the calculations of ZPE were presented in our previous study [53].

To simulate the behavior of the H₂ molecule in a homogeneous electron gas, the electrons are placed in an empty box with a compensating uniform positive background charge. First, a vacuum 10 × 10 × 10 Å supercell was constructed with fixed cell volume and shape. Next, a given number of electrons were embedded in the supercell, resulting in a specific homogeneous electron density with a compensating positive background charge. After that, two H atoms were added in the supercell at different H–H distance with different electron density and thus the total energy of the system as a function of H–H distance was calculated. The binding energy of a H₂ molecule with H–H distance of d_0 in a homogenous electron gas (with the electron density of n_0) can be obtained by,

$$E_{\text{H-H,ele}(n_0),d_0}^{\text{bind}} = E_{\text{2H,ele}(n_0)}^{\text{total}}|_{d=d_0} - E_{\text{2H,ele}(n_0)}^{\text{total}}|_{d=\infty}, \quad (1)$$

where the $E_{\text{2H,ele}(n_0)}^{\text{total}}|_{d=d_0}$ and $E_{\text{2H,ele}(n_0)}^{\text{total}}|_{d=\infty}$ are the total energy of the system containing two H atoms with H–H distance of d_0 and infinite distance (∞), respectively. From the above results, the largest binding energy of the H₂ molecule and optimal H–H distance in the different homogeneous electron density were obtained. It is important to note that a further correction induced by artificial long-range interaction between electrons in the system should be considered in the charged system due to finite-size effects within supercell calculations, as demonstrated in previous studies [54–56]. However, in our calculations, the binding energy of the H₂ molecule at a given electron density is evaluated by the difference between the total energy of the system with $d = d_0$ and $d = \infty$, as displayed in equation (1). So, a large part of the finite-size correction is canceled out by this subtraction, and the system size effect on the properties of the H₂ molecule in a homogeneous electron gas would not be significant (a detailed discussion of the finite-size effect on the properties of a H₂ molecule in a homogeneous electron gas are given in the supplementary data (stacks.iop.org/NF/59/106032/mmedia)).

3. Results and discussion

3.1. Dissolution of interstitial H in defect-free W

To examine the stability of interstitial H in bulk (defect-free) W, we calculated the H solution energies at possible interstitial sites, i.e. TIS and octahedral interstitial site (OIS), which can be expressed as,

$$E^{\text{sol}} = E_{\text{H+MW}} - E_{\text{MW}} - E_{\text{H}}^{\text{ref}}, \quad (2)$$

where $E_{\text{H+MW}}$ and E_{MW} are the energy of a unit cell including MW atoms with and without an interstitial H atom, respectively. $E_{\text{H}}^{\text{ref}}$ is the reference energy of H, corresponding to the one-half energy of the H₂ molecule in vacuum. Besides, in order to illustrate the effect of the atomic and volumetric relaxation on the H solution energy, three different relaxation conditions were employed, including the fully relaxed condition (corresponding to the relaxation of both the atomic position and the shape and volume of the supercell, i.e. ISIF = 3), partly relaxed condition (corresponding to the only atomic relaxation with fixed supercell shape and volume, i.e. ISIF = 2) and unrelaxed condition (corresponding to the fixed atomic position and the supercell volume and shape).

Table 1 displays the solution energy of the interstitial H at TIS and OIS in W with different relaxation methods. For the fully relaxed condition, the H solution energy at TIS is 1.01 (0.89) eV with (without) ZPE correction, which is 0.29 (0.39) eV lower than that at OIS. Moreover, there are two imaginary frequencies of H at OIS, indicating that the OIS is an unstable position of H in W. Thus, the TIS is the most favored occupation of interstitial H in bulk W, consistent with previous DFT results [10, 34, 35]. Generally, the H solution energies can be divided into three contributions, i.e. the ZPE contribution, MC and EC. The first term is the ZPE difference between a single H atom in W and a H atom in a H₂ molecule. The MC ($E_{\text{MC}}^{\text{sol}}$) is the deformation energy from a perfect W crystal to a H-induced distorted one, corresponding to the energy release of structure optimization after H removal, i.e. $E_{\text{MC}}^{\text{sol}} = E_{[(\text{H+MW})-\text{H}]}|_{\text{NSW}=1} - E_{\text{MW}}$,

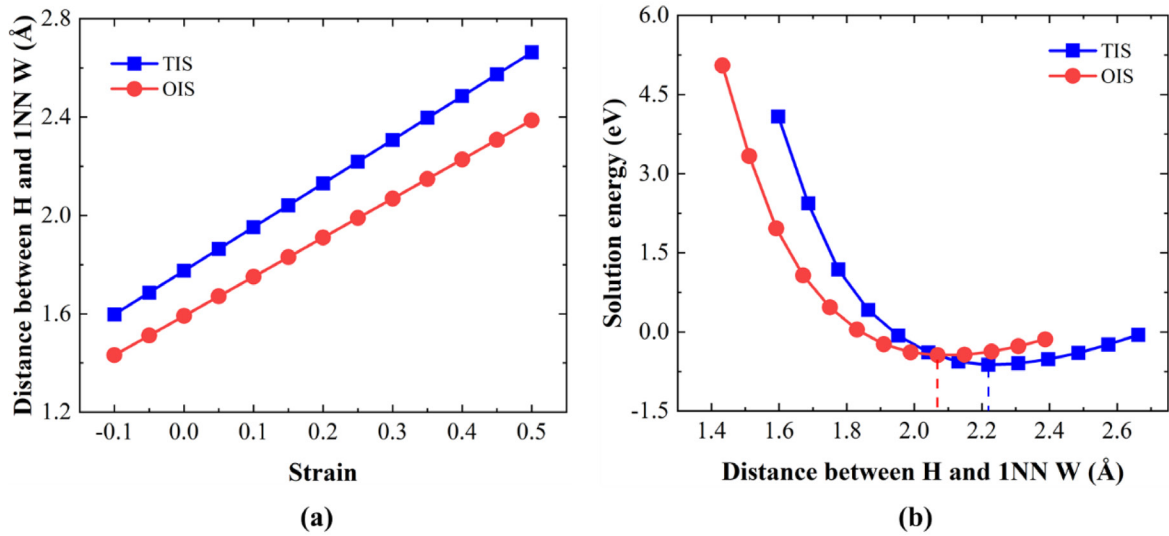


Figure 1. (a) 1NN distance of interstitial H with W under strain and (b) the corresponding H solution energy as a function of H–W distance.

where $E_{[(H+MW)-H]}|_{NSW=1}$ represents the total energy of the H-induced distorted supercell. As for the EC (E_{EC}^{sol}), it reflects the electronic interaction of H with neighboring host atoms, and can be calculated by subtracting the first and second contributions from the solution energy of H, namely $E_{EC}^{sol} = E^{sol} - E_{MC}^{sol} - E_{ZPE}^{sol}$. As illustrated in table 1, the EC is always larger than the MC and ZPE contribution, and takes up to 66% for H solution energy, implying that the electronic interactions of H with neighboring atoms are the dominating factor for the dissolution of interstitial H in W.

Interestingly, the relaxation methods will substantially affect the solution energy of H. As displayed in table 1, the solution energies of H under partly relaxed condition are basically consistent with those under fully relaxed condition. However, the H solution energy under unrelaxed condition is much larger than that under fully or partly relaxed condition. These suggest that the local atomic relaxation dominates the solution energy of H in W rather than the volumetric relaxation. To validate this speculation, we examined the variation of H–W distances after relaxation. Table 1 shows that the initial distance of H at TIS (OIS) with its first nearest neighboring (1 NN) W is 1.77 (1.59) Å, while it increases to 1.85 (1.75) Å after atomic relaxation (corresponding to the fully and partly relaxed condition). This implies that there is a repulsive interaction of interstitial H with its 1 NN W atom. Thus, it is a negative correlation between the H solution energy and 1 NN H–W distance, i.e. the smaller the 1 NN H–W distance, the higher the solution energy of H. Besides, the distances of H–W (2 NN) at both TIS and OIS are almost invariable under different relaxation conditions, suggesting the strong localization of H-induced atomic distortion.

In order to estimate the correlation between H–W distance and their electronic interaction, we further investigate the dissolution of interstitial H at TIS and OIS in the strained W.

Here, the isotropic strain is imposed on the body-center cubic (bcc) supercell, and the lattice constants (a_ϵ) of the strained system are determined by $a_\epsilon = (1 + \epsilon)a_0$, where ϵ and a_0 is the applied strain and the lattice constant of the strain-free system, respectively. Besides, to mimic the influence of atomic distance on the electronic interaction of H–W directly, the calculations are conducted with fixed atomic positions, corresponding to the fully fixed relaxation condition. Figure 1(a) shows the variation of H–W (1 NN) distance in the strained system. It can be found that the atomic distances of H–W for both TIS and OIS linearly increase with the increasing of hydrostatic tensile strain, but decrease with the increasing of hydrostatic compressive strain. Specifically, the H–W (1 NN) distance for TIS is 1.85 Å with the tensile strain of ~4%, which equals to that in strain-free W after atomic relaxation (see table 1). Figure 1(b) illustrates the solution energy of interstitial H in W under hydrostatic strain. In all cases, the solution energy of H in strained W decreases with increasing of H–W distance initially. After the lowest value of solution energy, it increases with increasing of H–W distance. This indicates that there is an optimal atomic distance for the electronic interaction of H–W in W. As demonstrated in figure 1(b), the optimal atomic distance of H–W in strained W is 2.22 (2.07) Å for the case of TIS (OIS) with the lowest solution energy of –0.62 (–0.44) eV. Such negative solution energies imply the attraction of H with neighboring W, which is different to the repulsion of H–W in strain-free W. Interestingly, the H solution energy at TIS under the strain of ~4% is ~0.54 eV, which almost equals the EC of H at TIS after relaxation (see table 1). Consequently, the stability of H is mainly determined by the electronic interaction of H with neighboring W atoms, which can be simply quantified by the atomic distance of H–W. In defect-free W, the interaction of H–W is repulsive due to the short atomic distance, corresponding to the positive value of

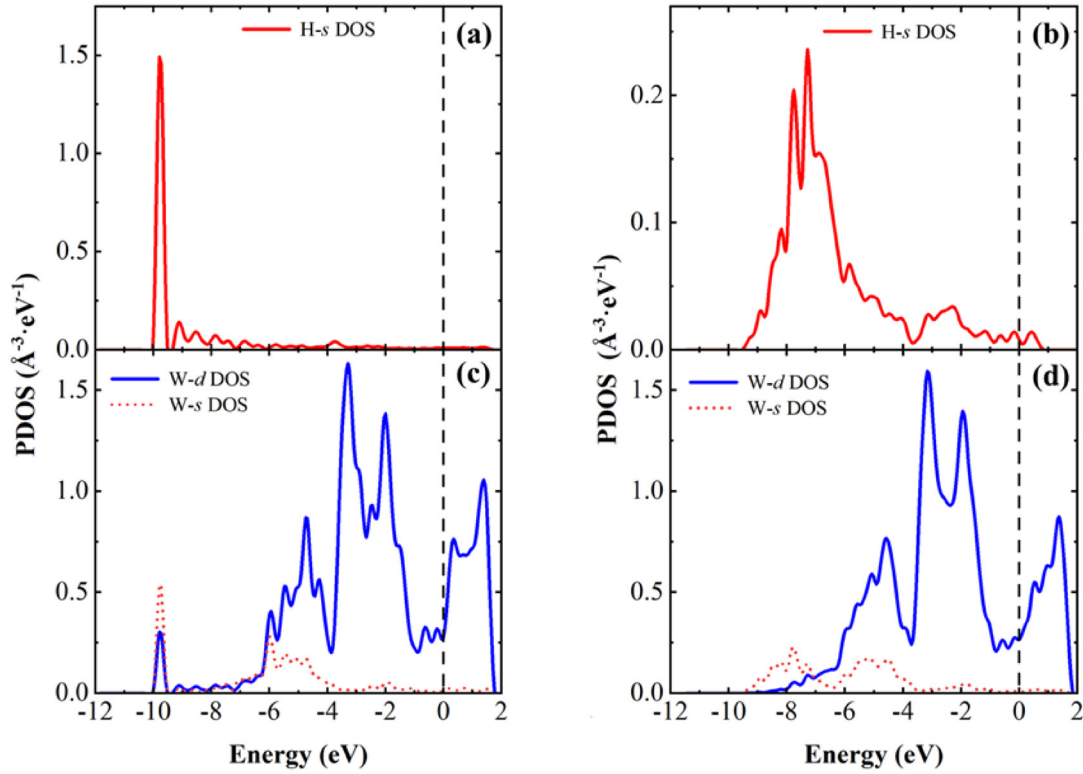


Figure 2. Projected density of states (PDOS) of H and its 1 NN W in W with and without a mono-vacancy. (a) and (c) H at TIS in defect-free W, and (b) and (d) H at a mono-vacancy in W.

H solution energy. It is expected that the presence of defects in W can provide the large available volume for H dissolution, reducing the solution energy of H.

3.2. Behavior of a single H in vacancy/VCS

3.2.1. Dissolution of a single H in a mono-vacancy. As demonstrated in previous studies [9, 10, 15, 28, 34], the vacancy-type defects can remarkably affect the behavior of H isotopes in W. Thus, to determine the dissolution behavior of H at a mono-vacancy in W, we examined the H solution energy at different sites in the vicinity of a mono-vacancy. Specifically, the most stable occupation of H at a mono-vacancy is an off-vacancy position (~ 1.27 Å to the vacancy center) and close to the OIS, as demonstrated in figure 3. Correspondingly, the solution energy of H with ZPE correction is -0.37 eV, ~ 1.38 eV lower than that at TIS in defect-free W (see table 1), suggesting the strong H trapping capability of mono-vacancy. This is well consistent with previous DFT calculations [34, 58].

The solution energy of H at a mono-vacancy can also be divided into three contributions. At the most stable site, the EC, MC and ZPE contribution for H solution energy is -0.37 , 0.00 and 0.00 eV, respectively. Similarly, the electronic interaction dominates the stability of H at a mono-vacancy in W and is mainly responsible for the reduction of H solution energy from 1.01 eV at TIS (see table 1) to -0.37 eV at a mono-vacancy. To accurately describe the electronic interaction H with neighboring host atoms, the PDOS for H and its 1NN W with and without a mono-vacancy are presented

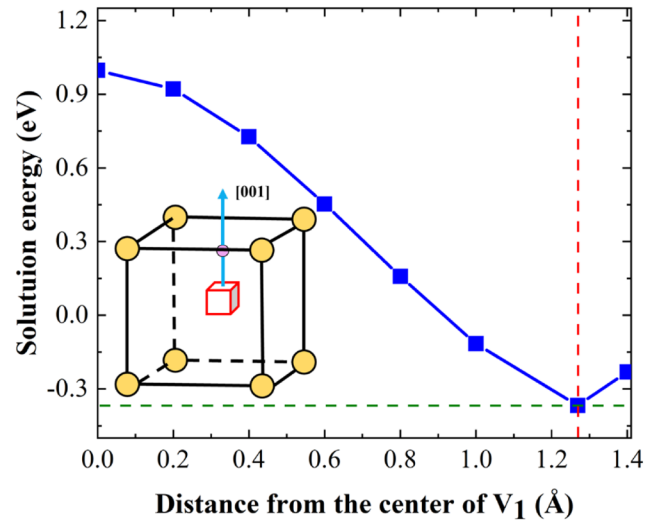


Figure 3. Solution energy of H at a mono-vacancy in W, as a function of the distance between H and the vacancy center.

in figure 2. Obviously, the PDOS of H and W in the mono-vacancy are substantially different to that at TIS, suggesting that vacancy can significantly affect the electronic interaction of H–W. For the case of H at TIS, there is only a single narrow peak around -10 eV for the H-s and W-s/W-d DOS, indicating the weak hybridization between H and 1 NN W [33]. As for H in the mono-vacancy, the H-s DOS are broadened, and similar structures appear for both H-s and W-s/W-d, suggesting the strong electronic hybridization of H with 1 NN W atoms. The same relationship has been found in other bcc metals, such as

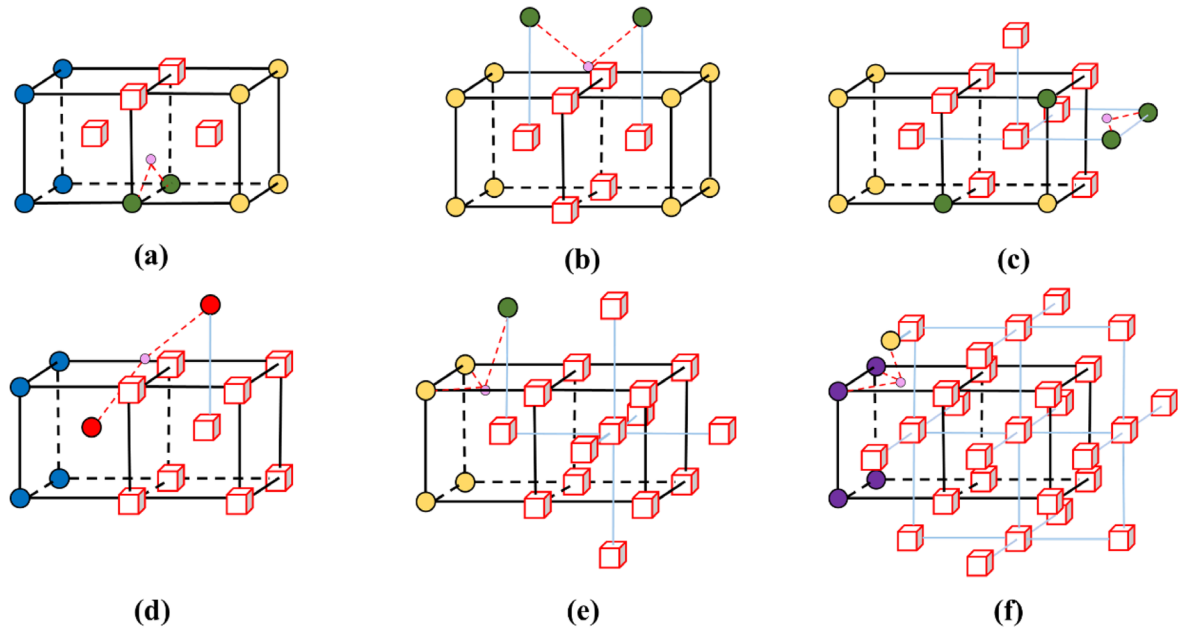


Figure 4. Stable configurations of a single H in VCs in W; (a) V_4 , (b) V_6 , (c) V_9 , (d) meta-stable V_9 ; (e) V_{15} and (f) V_{27} . H atoms are denoted by the small pink balls, and the vacancies by the red square. Blue, yellow, green, purple and red balls denote W atoms with the coordination number of 8, 7, 6, 5 and 4, respectively. Red dotted lines connect the H atom and its neighboring W atoms.

Fe and Mo [59, 60]. Such a vacancy-enhanced hybridization is originated from the variation of the electronic states of W, which will be directly discussed in section 3.2.2.

To illustrate the relative stability of H in the vicinity of the mono-vacancy, we further calculated the solution energy of H at different sites in the mono-vacancy. Here, a H atom is set at the positions along the [001] direction with different distances to the vacancy center, and the solution energies of H are displayed in figure 3. For the case of H at the vacancy center, the H solution energy reaches up to 1.00 eV. Such a large solution energy is comparable with that of H at TIS in defect-free W. Besides, the solution energies of H decrease with increasing of H-vacancy center distance, from 1.00 eV with H-vacancy center distance of 0.00 Å to −0.37 eV with H-vacancy center distance of 1.27 Å. After that, the H solution energy increases with increasing of H-vacancy center distance. This ‘down and up’ trend can be simply understood by the electronic interaction of H with 1 NN W atoms. For the case of H at the vacancy center, the distance of H–W(1 NN) is 2.73 Å, much longer than the optimal electronic interaction distance of H–W (2.15 ± 0.08 Å), as shown in figure 1. These suggest that the attraction of H with W drives H to move towards the neighboring W atoms, reducing the H–W distance and the H solution energy. As for the most stable site, the H atom is surrounded by four W atoms with the H–W distance of ~2.26 Å, which is the same as the H–W optimal electronic interaction distance given in figure 1. Therefore, the occupation of single H in a mono-vacancy mainly depends on the H–W distance.

3.2.2. Trapping behavior of H in VCs. Next, to investigate the trapping behavior of a single H atom in small VCs (V_m) in W, we calculated the H trapping energy in VCs, which can be given by,

$$E^{\text{trap}} = E_{\text{H}+(M-m)\text{W}} - E_{(M-m)\text{W}} - E_{\text{H}+\text{MW}} + E_{\text{MW}}, \quad (3)$$

where $E_{\text{H}+(M-m)\text{W}}$ and $E_{(M-m)\text{W}}$ are the energy of a unit cell with a H– V_m and V_m cluster in W, respectively. Negative trapping energies represent that the H atom energetically prefers to be trapped by VCs. As reported in previous studies [47, 61, 62], although the binding energy of di-vacancy in W is negative, the binding energy of VCs ($m > 3$) is positive and increases with the increasing of cluster size, indicating the attractive interaction between vacancies for VCs in W. Here, in order to obtain the most stable configuration of V_m clusters in W, we constructed the V_m clusters from the most stable configuration of V_4 (as reported in [62–64]), and the subsequent vacancy is set at the different 1 NN sites of VCs. Besides, some high-symmetric configurations have also been taken into account. After that, we calculated the total energy of different configurations to determine the most stable one (the variation of lattice constant and supercell volume induced by VCs are presented in table S1). Figure 4 displays the most stable configurations of a single H at small VCs in W. Note that a high-symmetric and metastable configuration of V_9 cluster (V_9^m) has also been considered, as illustrated in figure 4(d), since this structure is very representative of VCs. Apparently, the inner surfaces of VCs provide the optimal occupation of H rather than the centers of VCs, which is rationalized by the interaction of H with neighboring W atoms. Moreover, different to the most stable site of a single H at the mono-vacancy, which in VCs is close to the TIS, and the corresponding 1 NN H–W distances range from 1.88 – 1.96 Å.

Figure 5(a) shows the trapping energies of H in small VCs in W. Note that the H trapping energy is always negative, implying the strong trapping effect of VCs on H. However, the H trapping energies are significantly different in different VCs. As presented in figure 5(a), the H trapping energy is −1.38 eV

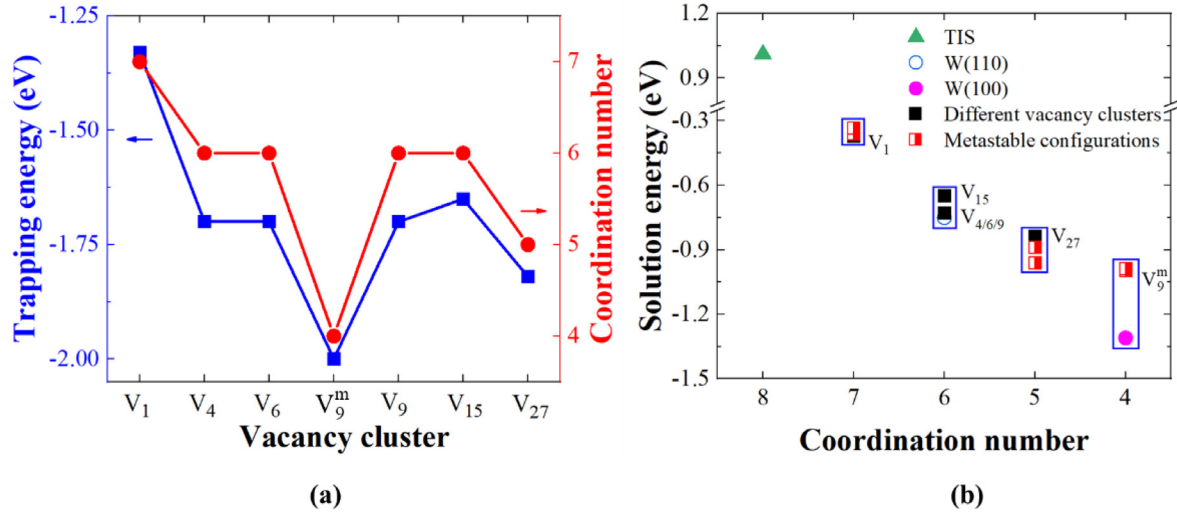


Figure 5. (a) Trapping energy (with ZPE correction) of H in different VCs in W and the corresponding number of coordination atoms of neighboring W atoms. (b) Solution energy (with ZPE correction) of H as a function of the coordination number of neighboring W atoms.

(−1.26 eV) at a mono-vacancy with (without) ZPE correction, while the lowest H trapping energy in VCs is −2.00 eV (−1.87 eV) in a V_9^m cluster with (without) ZPE correction. Such a significant energy variation suggests that the stability of H is very sensitive to the size of the VCs. Specifically, the H trapping energies in the VCs are much lower than that in a mono-vacancy, indicating that the trapping capability of VCs for H is stronger than that of a mono-vacancy. As discussed in sections 3.1 and 3.2.1, the electronic interactions of H with neighboring W are mainly responsible for the stability of H, which is related to the electronic states of W. Furthermore, the electronic states of W should be determined by the local atomic environment, and thus the neighboring W atoms are categorized by the number of coordination atoms. Due to the bcc structure, the coordination number of W in defect-free materials is eight. However, the presence of VCs will reduce the coordination number of W atoms, as presented in figure 4, and thus affect the dissolution of H nearby. This is evidenced by figure 5(a), in which the trapping energy of H is almost proportional to the coordination number of neighboring W atoms.

To further verify this speculation, some metastable configurations of H in VCs and W surfaces, including W (100) and (110) surface, are considered to calculate the H solution energy in W with different coordination number of neighboring W atoms. Here, we examined the solution energy of H at the W surface to approximate the dissolution of H in large VCs/voids in W. Figure 5(b) displays the solution energies of H as a function of the coordination number of neighboring W atoms. Obviously, there is a distinct difference for the H solution energy, which is strongly related to the coordination number of W. For the case of the coordination number of eight, the H solution energy is 1.01 (1.30) eV at TIS (OIS) in defect-free W. The H solution energy decreases monotonically with decreasing of the coordination number of neighboring W atoms. For the interaction of H with seven-, six-, five- and four-coordination-number W, the corresponding solution energy of H is −0.37 to −0.33 eV, −0.75 to −0.69 eV, −0.96

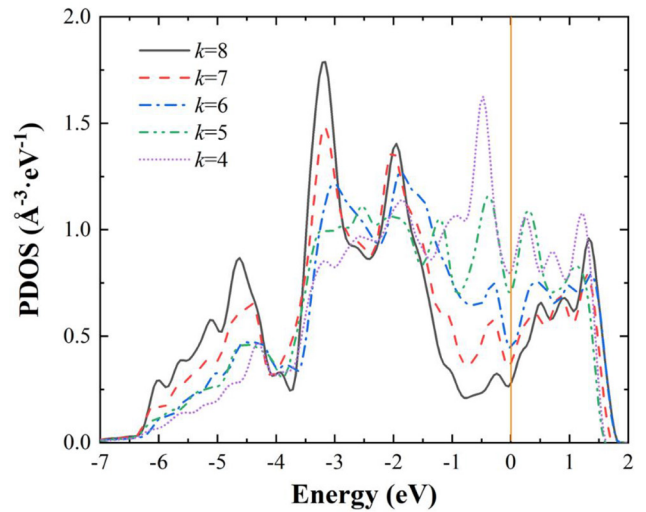


Figure 6. d-projected DOS of W with different coordination number. k represents the coordination number of W.

to −0.84 eV and −1.31 to −0.99 eV, respectively. Such a remarkable reduction of H solution energy suggests that the coordination number of W atoms affects the dissolution of H nearby, i.e. the lower the coordination number of W, the lower the H solution energy. It should be noted that the lowest H solution energy is −1.31 eV, corresponding to the dissolution of H at the W (100) surface. Besides, the slight energy difference at the same coordination number is rationalized by the different atomic configurations. For example, although the coordination number of neighboring W atoms is six for both $V_4/V_6/V_9$ and V_{15} , the solution energy of a single H in V_{15} is slightly higher than that in $V_4/V_6/V_9$. This is because only one six-coordination-number W atom interacts with H in H- V_{15} complex (see figure 4(e)), while there are two bonds of H with six-coordination-number W atoms in H- V_4 /H- V_6 /H- V_9 complex (see figures 4(a) and (c)).

Physically, the variation of coordination number can change the electronic states of W, and thus influence the electronic

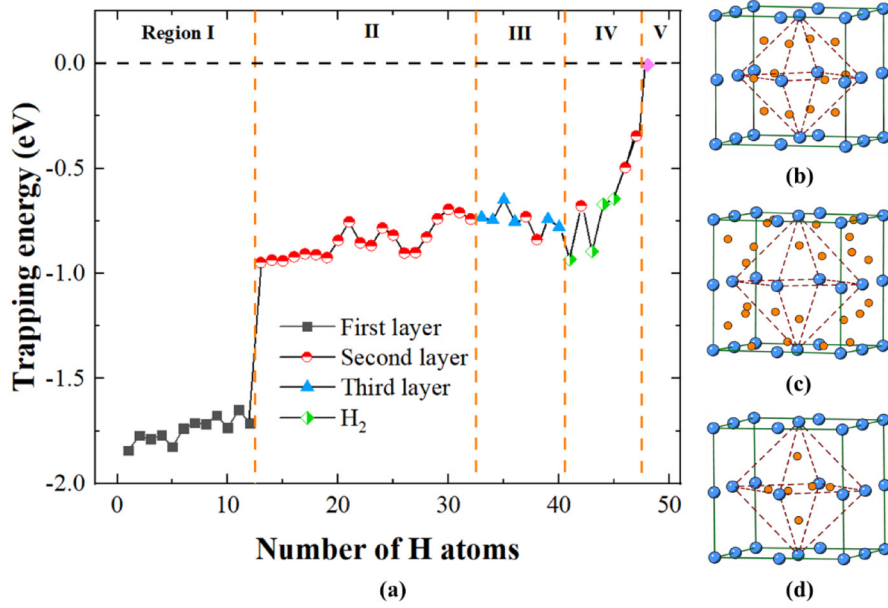


Figure 7. (a) Trapping energy per H as a function of the number of H atoms in a $H_n-V_9^m$ complex. Atomic structure of H in a V_9^m cluster at the first, second and third layer is displayed in (b) and (d), respectively.

interaction of H with W, which has been observed in other materials [62, 65, 66]. To quantitatively evaluate the effects of the coordination number on the electronic structure of W, the d -projected DOS for W with a different coordination number in bcc W are presented in figure 6 (for comparison, the W- d DOS in the strained system and related discussions are given in the supplementary data). As illustrated in previous studies [67, 68] and our calculations, the PDOS of bulk W (corresponding to the coordination number of eight) has a bimodal shape with a marked pseudo-gap responsible for the stability of the bcc structure close to half-band filling. More importantly, with the reduction of the coordination number, the number of electronic states for W in the vicinity of the Fermi level increases, while the number of electronic states far from the Fermi level decreases. This will lead to a substantial increase of band-energy contribution to the total energy in comparison with bulk W atoms (since the Fermi level of the W atoms is closer to the minimum of the pseudo-gap), i.e. the larger the reduction of the coordination number, the larger the band-energy contribution to the total energy. Such variation is consistent with the previous studies for the dislocation in bcc W [67] and Mo [68]. Thus, the VCs can reduce the coordination number of neighboring W atoms, promoting their electronic states and resulting in the instability of W. These promoted electrons of W are strongly attracted by H, enhancing the electronic interaction of H with W. Consequently, the reduction of the coordination number causes the instability of W, which strengthens the H-W attraction, leading to the reduction of H solution/trapping energy (a detailed discussion of the stability of H in W by referring to the electron density, H-W distance and coordination number of neighboring W atoms is presented in the supplementary data).

3.3. Behavior of multiple H atoms in VCs

3.3.1. Dissolution of H at the inner surface of VCs. Considering the strong trapping effects of VCs for H, the isolated H atoms will segregate to the VCs in W, resulting in the aggregation of H atoms. Here, taking V_9^m as an example (corresponding to the lowest H trapping energy and the representative configuration of VCs), we investigated the dissolution of multiple H atoms in VCs. The most stable configurations of $H_n-V_9^m$ complexes were constructed from $H_1-V_9^m$ clusters (see figure 4(d)), and the future H atoms are introduced one by one and set at the different sites in the clusters, including the inner surface and the center of the VCs. Some high-symmetric configurations have also been taken into account. After that, the total energy for different configurations was examined, and the lowest total energy corresponds to the most stable one (the variation of lattice constant and supercell volume induced by the additional H atoms are presented in table S1). Based on the most stable structures, we further calculated the sequential trapping energy of H in $H_n-V_9^m$ complexes, which can be obtained as follows:

$$E_n^{\text{trap}} = E_{nH+(M-9)W} - E_{(n-1)H+(M-9)W} - E_{H(\text{TIS})+MW} + E_{MW}, \quad (4)$$

where $E_{nH+(M-9)W}$ and $E_{(n-1)H+(M-9)W}$ are the energy of a unit cell containing a $H_n-V_9^m$ and $H_{(n-1)}-V_9^m$ complex, respectively.

Figure 7(a) illustrates the sequential H trapping energy in $H_n-V_9^m$ complexes, and some typical structures of multiple H atoms are present in figures 7(b)–(d). Note that the sequential H trapping energies basically increase with the increasing of H numbers, implying that the pre-existing H will weaken the trapping effects of the VCs on H. Specifically, based on the

sequential trapping energy and H-occupied position, the dissolution of multiple H atoms in a V_9^m cluster should be divided into five regions. For the first region, the sequential H trapping energy is -1.87 to -1.65 eV, corresponding to the dissolution of the 1st–12th H atoms. These H atoms occupy 12 equivalent positions at the inner surface of V_9^m cluster (~ 2.44 Å to the center of the cluster), as demonstrated in figure 7(b), and they both interact with two four-coordination-number W atoms (see figure 4(d)), resulting in similar values of H trapping energy. As for the second region, the trapping energy of H ranges from -0.95 to -0.69 eV, corresponding to the dissolution of 13th–32nd H atoms, which is ~ 0.90 eV higher than that in the first region. Such a remarkable variation of H trapping energy indicates the different H-occupied position. As displayed in figure 7(c), there are 24 equivalent positions (~ 3.79 Å to the VC center) for the occupation of H atoms in the second region, and the interaction of H with one four-coordination-number W determines the H trapping energies. Similarly, the slight increase of H solution energy is due to the repulsion between the H atoms. In the third region, the H atoms form an octahedron (double pyramid) in V_9^m , as illustrated in figure 7(d), and their trapping energy varies from -0.78 to -0.65 eV. From the above results, a distinct layered configuration for multiple H atoms at the inner surface of the V_9^m cluster is observed. The off-VC-center distance is 2.43 – 2.45 Å, 3.49 – 4.03 Å and 1.55 – 1.60 Å for the first, second and third layer, respectively. Besides, the closest 1NN distance of H–H pair in these regions is ~ 1.65 Å, much longer than that of the H_2 molecule (~ 0.75 Å). However, in the fourth region, the stable H_2 molecules with the H–H distance of 0.83 – 0.85 Å are observed. Specifically, the trapping energy of the 41st (corresponding to the formation of the 1st H_2 molecule), 43rd (for the 2nd H_2 molecule), 44th (for the 3rd H_2 molecule) and 45th (for the 4th H_2 molecule) H atom is -0.93 , -0.89 , -0.67 and -0.64 eV, respectively. Such negative trapping energies suggest that these H atoms energetically prefer to segregate from bulk W to the VCs, leading to the formation of stable H_2 molecules. More detailed analyses of the formation of the H_2 molecule are presented in section 3.3.2. As for the 48th and subsequent H atoms (corresponding to the fifth region), the trapping energy of H is practically zero (or even positive). Therefore, the maximum H number in a the V_9^m cluster is 47. It should be noted that there are ~ 12 H atoms trapped by a mono-vacancy at 0 K [34], and thus the maximum H-to-vacancy ratio in a mono-vacancy (~ 12) is much higher than that in a V_9^m cluster (~ 5.2). Similar features for the dissolution of multiple H atoms in W have also been observed in a V_{15} cluster (see figure S3 for details).

As mentioned in section 3.2.2, the VCs can reduce the coordination number of W and destabilize its electrons, enhancing the attraction of H–W and facilitating the dissolution of H. Nevertheless, the pre-existing H atoms basically increase the solution energy of subsequent H even with the same coordination number of W. As presented in figure 7, the trapping energy of the 13th H in V_9^m is -0.95 eV, corresponding to the interaction of H with four-coordination-number W, while that of a single H in V_9^m is -1.87 eV with the same coordination number of W. There are two possible interpretations

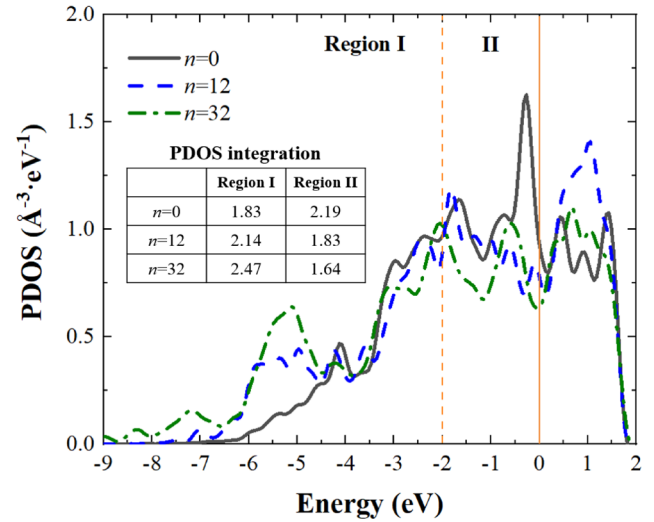


Figure 8. d -projected DOS of W with minimum coordination number in the vicinity of H_n - V_9^m complexes.

for the increase of H trapping energy. The first explanation is due to the repulsion between H atoms. However, atomic structure shows that the 1NN distance between the 13th H and remaining H atoms is 2.20 Å. Such a long atomic distance implies the weak repulsion of the H–H pair. The second interpretation is that the pre-existing H atoms can also change the electronic states of neighboring W atoms, and thus affect the interaction of subsequent H with W. To explore this possibility, we determined the d -projected DOS of W with the coordination number of four in pure V_9^m , H_{12} - V_9^m and H_{32} - V_9^m complexes. As displayed in figure 8, the pre-existing H atoms can modify the electronic states of W, especially in the vicinity of the Fermi level. With the increasing of H numbers, the W- d DOS substantially decrease in the energy region close to the Fermi level (-2 to 0 eV), while increase in the energy region far away from the Fermi level (-9 to -2 eV), leading to the decrease of the band-energy contribution to the total energy. This indicates that the pre-existing H atoms can stabilize the electrons of W, weakening the attraction of H with W and increasing the solution/trapping energy of subsequent H.

3.3.2. Formation of H_2 molecules in VCs. As the initial stage and driving force for the growth of H bubbles, the H_2 molecule is an interesting and important characteristic to identify the H-induced damage. However, the formation of the H_2 molecule in vacancy-type defects in W is still under debate, because the available volume provided by a mono-vacancy is very small [10, 15, 32, 34]. According to our calculations, it is clearly evidenced that the H_2 molecules can be formed in the VCs in W, and a V_9^m cluster can accommodate four H_2 molecules at 0 K, as demonstrated in figure 7(a). Here, only when the binding energy of two H atoms (forming a H_2 molecule) are positive and the corresponding H–H distance is comparable with that of a H_2 molecule in vacuum (~ 0.75 Å), is the corresponding H–H pair considered to be a H_2 molecule. Interestingly, the binding energies of H_2 molecules in a V_9^m cluster are 0.77 , 0.70 , 0.31 and 0.20 eV with the H–H distance of 0.83 , 0.83 , 0.84 and 0.85 Å, respectively (the detailed

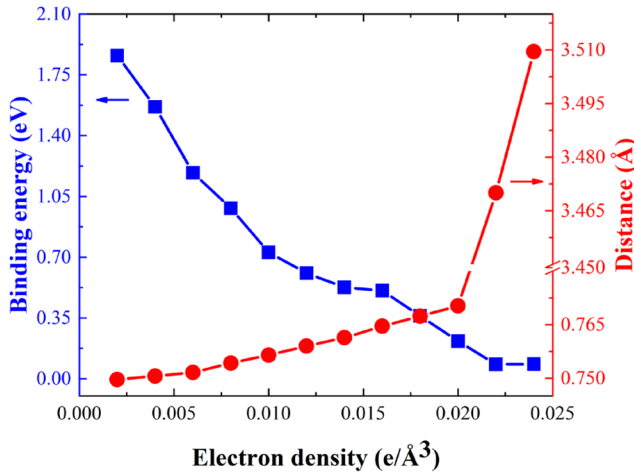


Figure 9. Largest binding energy and optimal atomic distance of the H_2 molecule in the homogeneous electron gas.

calculation for the binding energy of the H_2 molecule in a V_9^m cluster is presented in the supplementary data). Namely, with increasing H numbers, the binding energies of H_2 molecules decrease and the corresponding H–H distances increase slightly. Also, it should be noted that the binding energies of the H_2 molecules in a V_9^m cluster are much lower than that in vacuum (~ 4.55 eV). This can be attributed to the influence of neighboring W atoms, which weakens the attraction of the H_2 molecule. Moreover, based on the equation of state of the H_2 molecules, the pressure in a V_9^m cluster induced by four H_2 molecules is estimated as 17.46 GPa (the detailed estimation for the pressure of the H_2 molecules in a V_9^m cluster is given in the supplementary data).

To explore the underlying physics for the formation of the H_2 molecule in the VCs in W, the properties of the H_2 molecule in the homogeneous electron gas have been determined, because the electronic environment in metals can be roughly approximated by the homogeneous electron gas. Figure 9 shows the largest binding energy of the H_2 molecule and the corresponding optimal atomic distance in the homogeneous electron gas with different electron density. For the electron-free environment (or vacuum), the largest binding energy of the H_2 molecule is 4.55 eV at the atomic distance of 0.75 Å. Then, the binding energy (atomic distance) of the H_2 molecule monotonically decreases (increases) with the increasing of the electron density. Specifically, when the electron density is larger than $0.02 e/\text{\AA}^3$, the binding energy of the H_2 molecule almost converges to zero and the corresponding H–H distance can reach up to ~ 3.5 Å. These results suggest that the free electrons will interact with H atoms, resulting in the weakening effects on the attraction of the H_2 molecule. Once the electron density exceeds the critical value ($\sim 0.02 e/\text{\AA}^3$), the H_2 molecule will be dissociated.

From the above analysis, the properties of the H_2 molecule are strongly related to the environmental electron density. Thus, we further examined the electron density in a V_9^m cluster with different numbers of H atoms. As illustrated in figure 10, considering the optimal distance (~ 0.75 Å) of the H_2 molecule, the electron density at the VC center in pure V_9^m

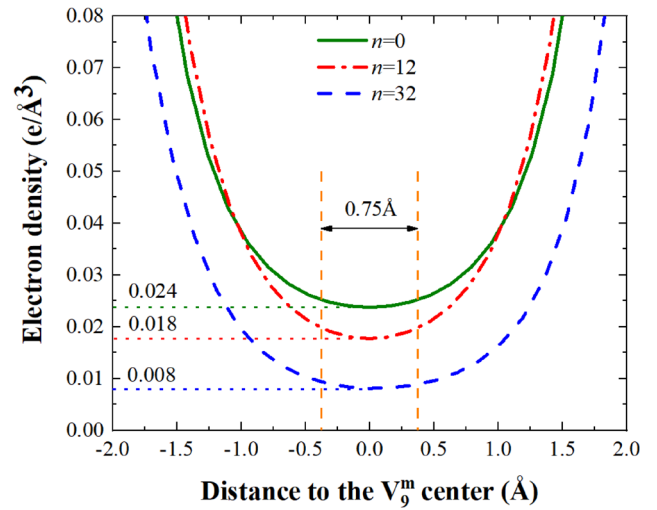


Figure 10. Electron density curve along the $\langle 100 \rangle$ direction in the $\text{H}_n\text{-}V_9^m$ complexes in W.

(without H atoms) is $0.024\text{--}0.025 e/\text{\AA}^3$. This is higher than the critical electron density ($\sim 0.02 e/\text{\AA}^3$) of the H_2 molecule in the homogeneous electron gas (see figure 9), implying the instability of the H_2 molecule in pure V_9^m . Nevertheless, the presence of H atoms at the surface of the VCs will reduce the electron density in the center of the VCs. For example, the electron density at the center in the $\text{H}_{12}\text{-}V_9^m$ complex is $0.018\text{--}0.019 e/\text{\AA}^3$. When the 32 H atoms are introduced in a V_9^m cluster (see figure 7), the electron density of the center of the VC is $0.008\text{--}0.009 e/\text{\AA}^3$, much lower than the critical electron density of the H_2 molecule, and thus the formation of the H_2 molecule is possible. Consequently, the dissolution of H atoms at the inner surface of the VCs will provide a shielding effect for the electrons of W, leading to the reduction of electron density at the center of the VCs and facilitating the formation of the H_2 molecule.

3.4. Retention of H in the VCs in W: a temperature-dependent desorption

According to our calculations, the VCs can significantly affect the behavior of H in W, which is consistent with experimental observations [15, 16, 37, 69, 70]. Specifically, the H trapping energy in the VCs in W is in the range of -2.00 to -1.65 eV, much lower than that at a mono-vacancy (~ -1.38 eV), suggesting that the VCs are strong trapping centers for H, especially under neutron-irradiated condition. To evaluate the influence of the VCs on H isotope retention, we examined the temperature (T_{max}) of H desorption with maximum de-trapping rates. As demonstrated in previous studies [33, 37, 71], the T_{max} can be evaluated by the Polanyi–Wigner equation, which can be expressed as,

$$\frac{E^{\text{de-trap}}}{kT_{\text{max}}^2} = \frac{\nu}{\beta} \exp\left(\frac{-E^{\text{de-trap}}}{kT_{\text{max}}}\right), \quad (5)$$

where $E^{\text{de-trap}}$ is the de-trapping energy, corresponding to the migration energy barrier (E^m) of H plus the opposite value of H trapping energy ($-E^{\text{trap}}$), i.e. $E^{\text{de-trap}} = E^m - E^{\text{trap}}$. The

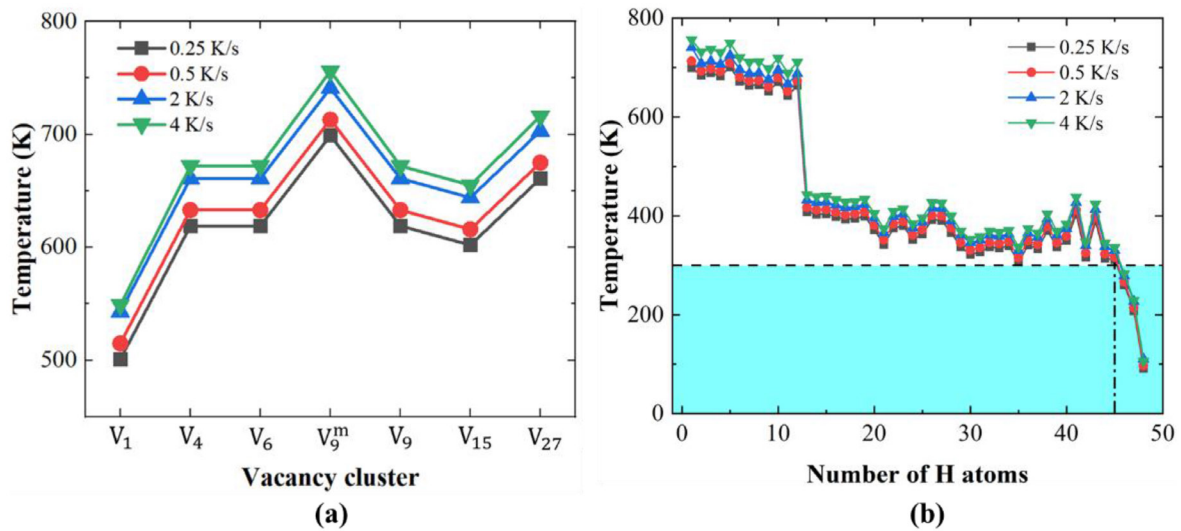


Figure 11. Maximum release temperature of H in (a) H₁-VC and (b) H_n-V₉^m complexes. Heating rates are set to be 0.25, 0.5, 2 and 4 K s⁻¹.

calculated migration energy barrier of H in defect-free W is 0.19 eV with ZPE correction [53]. k is the Boltzmann constant. The heating rate (β), as an important parameter for TDS experiments, can affect the maximum release temperature of H in W and is naturally inserted into the Polanyi–Wigner equation. Indeed, according to our calculation, the H release temperature can be reduced by about 35 K when the heating rate decreases by an order of magnitude. Such variation is consistent with previous DFT studies [33, 37, 71] and TDS experiments [72–74]. Furthermore, in order to mimic the influence of heating rates on the TDS measurements, four different heating rates (0.25, 0.5, 2 and 4 K s⁻¹) are considered, which are extensively employed in the experiments [17, 27, 73–76]. ν is the attempted frequency for the de-trapping of H, which is estimated as the mean value of H vibration and can be calculated by first-principles calculations.

It is important to note that if the activation energy of vacancy dissociation (corresponding to the de-trapping energy of vacancy, e.g. $H_n V_m \rightarrow H_n V_{m-1} + V$) is approximate to that of the H desorption (e.g. $H_n V_m \rightarrow H_{n-1} V_m + H$), the vacancy dissociation should also be considered in the thermal desorption process. As mentioned above, the de-trapping energy is the migration energy barrier *plus* the opposite value of trapping energy. For the case of vacancy dissociation, the migration energy barrier of vacancy is calculated to be 1.70 eV, inconsistent with previous studies [62, 77, 78]. Furthermore, the trapping energy of a mono-vacancy in H–V complexes is lower than –0.75 eV, and more importantly, the vacancy trapping energy decreases with the increasing of H numbers (see table S2). These results suggest that the de-trapping energy of vacancy from H–V complexes is larger than 2.45 eV, while the maximum de-trapping energy of H is only 2.19 eV, suggesting that the possibility of vacancy dissociation is much lower than that of H desorption. Therefore, the H de-trapping process should be mainly responsible for the thermal desorption of H–V complexes in W, and the vacancy dissociation processes have not been considered in the following part.

The maximum release temperatures of H in the VCs in W are displayed in figure 11(a). Although the maximum release temperatures of H are reduced by about 57 K with the decreasing of the heating rate from 4 to 0.25 K s⁻¹, the variation trend of maximum release temperature barely changes under different heating rates. Besides, taking the heating rate of 4 K s⁻¹ as an example, the maximum release temperature increases with the increasing of the size of the VCs initially, from 549 K at the mono-vacancy to 756 K in a V₉^m cluster. After that, the maximum release temperature is 655 and 716 K in a V₁₅ and V₂₇ cluster, respectively. This trend is consistent with the variation of H trapping energy in the VCs (see figure 5(a)). Specifically, the de-trapping temperatures of H in the VCs are much larger than that at a mono-vacancy, suggesting that the aggregation of vacancies in W can enhance the trapping capability of H. Furthermore, the maximum release temperature of multiple H atoms in a V₉^m cluster gives the different results. As presented in figure 11(b), the H desorption temperature in H_n-V₉^m complexes can be divided into three regions, i.e. 1st–12th H atoms, 13th–45th H atoms and subsequent H atoms. In the first region, the maximum release temperatures of H are 689–756 K, corresponding to the first-layer H in V₉^m (see figure 7(b)). In the second region, the de-trapping temperatures of H are 300–443 K, which are higher than RT. As for the subsequent H atoms, the maximum release temperatures are lower than RT, implying the weak trapping capability of H. These results suggest that the maximum H number in a V₉^m cluster in W is 45 at RT. It is well documented that there are ~six H atoms at a mono-vacancy in W at RT [33, 38], and thus the maximum H-to-vacancy ratio at RT in a V₉^m cluster (~5) is 16.7 % less than that in a mono-vacancy (~6).

By means of TDS measurements, the desorption of H isotopes in W have been examined in many experimental studies. For example, Tyburska *et al* [29, 79] and Alimov *et al* [80] explored the desorption of D in W after exposure to a low-energy (200 eV in [29, 79] and 38 eV in [29, 79, 80]) and high-fluence (~10²⁴ D m⁻² in [29, 79] and ~10²⁶ D m⁻² in [29, 79,

80]) D plasma at low temperature (320–335 K). Two distinct peaks of the H desorption temperature were observed (with the heating rates of 0.5 K s^{-1} in [80] and 1.2 K s^{-1} in [29, 79]), near 600 and 450 K, corresponding to the de-trapping of H from a mono-vacancy (see figure 11(a)) and other shallow trapping sites. Interestingly, with the increasing of the temperature or fluence, obvious peaks appeared around high temperature (650–900 K). Furthermore, Tyburska *et al* [29, 79] and Zibrov *et al* [73, 74] determined the thermal desorption of D in W (with the heating rates of 1.2 K s^{-1} in [29, 79] and $0.25\text{--}4 \text{ K s}^{-1}$ in [73, 74]) with the pre-irradiation of high-energy particles (5.5 MeV W^+ in [29, 79] and 10 keV D^+ in [73, 74]). Also, the high-temperature peak ($\sim 700 \text{ K}$) with the maximum desorption rate of D was observed. Since both of the high irradiation temperature, high H isotope concentration and pre-irradiation of high-energy particles will facilitate the formation of VCs, the desorption of H isotopes at high temperature ($\sim 700 \text{ K}$) can be attributed to the VCs in W. The calculated de-trapping temperatures of H in the VCs (see figure 11) are quantitatively consistent with experimental results [29, 73, 74, 79–81]. Therefore, our calculations suggest that the VCs play a critical role in the retention and desorption of H isotopes in W-PFM, especially under extremely irradiated condition (high temperature, high fluences, pre-irradiation, etc), which provides an important reference to evaluate the properties and performance of W-PFM.

4. Conclusions

By using the first-principles method, we have systematically explored the dissolution and aggregation of H in vacancy/VCs in W. The stability of H is mainly determined by the electronic interaction of H with neighboring W atoms, which can be quantified by the atomic distance. Due to the short atomic distance of H–W, the interaction of H–W in defect-free W is repulsive, resulting in the high solution energy of H. However, the presence of vacancies can provide a large available volume for H dissolution, leading to the transition of the H–W interaction from repulsion in perfect crystal to attraction in vacancy. Besides, to optimize the H–W interaction ($\sim 2.15 \text{ \AA}$), the H atoms energetically prefer to occupy the inner surface rather than the vacancy center of a mono-vacancy.

Furthermore, VCs can significantly affect the behavior of H in W, and the corresponding trapping energy is in the range of -2.00 to -1.65 eV , much lower than that at a mono-vacancy ($\sim -1.38 \text{ eV}$). Specifically, the H solution/trapping energy in VCs can be well categorized by the coordination number of neighboring W atoms, i.e. the lower the coordination number of W, the stronger the H–W attraction and the lower the H solution/trapping energy. This is rationalized by the instability of W electrons induced by the reduction of the coordination number, which strengthens the attraction of H with W. Furthermore, a distinct layered configuration is observed for multiple H atoms at the inner surface of a V_9^m cluster in W. As for the continual dissolution of H, stable H_2 molecules are formed with positive binding energies. This is due to the shielding effect of pre-existing H atoms at the inner

surface of the VCs, which reduces the electron density of the center of the VCs and facilitates the formation of the H_2 molecule. Furthermore, the predicted release temperature of H in VCs varies from 650–750 K, giving an excellent correspondence with the available TDS experiments. These results reveal the critical role of VCs on the behavior of H isotopes, which provides a good reference to understand TDS measurements in recent experiments and to evaluate the evolution and retention of H isotopes in W-PFM.

Acknowledgment

This research is supported by the National Natural Science Foundation of China under Grant No. 11675011.

ORCID iDs

Hong-Bo Zhou  <https://orcid.org/0000-0001-5585-6154>

L. Cheng  <https://orcid.org/0000-0002-3537-784X>

References

- [1] Pitts R., Carpentier S., Escourbiac F., Hirai T., Komarov V., Ligo S., Kukushkin A., Loarte A., Merola M. and Naik A.S. 2013 *J. Nucl. Mater.* **438** S48–56
- [2] Hirai T., Escourbiac F., Carpentier-Chouchana S., Fedosov A., Ferrand L., Jokinen T., Komarov V., Kukushkin A., Merola M. and Mitteau R. 2013 *Fusion Eng. Des.* **88** 1798–801
- [3] Blagoeva D., Opschoor J., Van der Laan J., Sârbu C., Pintsuk G., Jong M., Bakker T., Ten Pierick P. and Nollés H. 2013 *J. Nucl. Mater.* **442** S198–203
- [4] Neu R., Riesch J., Coenen J., Brinkmann J., Calvo A., Elgeti S., García-Rosales C., Greuner H., Hoeschen T. and Holzner G. 2016 *Fusion Eng. Des.* **109** 1046–52
- [5] Causey R.A. and Venhaus T.J. 2001 *Phys. Scr.* **2001** 9
- [6] Wang W., Roth J., Lindig S. and Wu C.H. 2001 *J. Nucl. Mater.* **299** 124–31
- [7] Frauenfelder R. 1969 *J. Vac. Sci. Technol.* **6** 388–97
- [8] Alimov V.K., Shu W.M., Roth J., Sugiyama K., Lindig S., Balden M., Isobe K. and Yamanishi T. 2009 *Phys. Scr. T* **138** 014048
- [9] Eleveld H. and Veen A.V. 1992 *J. Nucl. Mater.* **191–4** 433–8
- [10] Liu Y.L., Zhang Y., Zhou H.B., Lu G.H., Liu F. and Luo G.N. 2009 *Phys. Rev. B* **79** 172103
- [11] Ohsawa K., Goto J., Yamakami M., Yamaguchi M., Yagi M. and Osawa K. 2010 *Phys. Rev. B* **82** 3987–96
- [12] Grigorev P., Terentyev D., Dubinko V., Bonny G., Oost G.V., Noterdaeme J.M. and Zhurkin E.E. 2015 *Nucl. Instrum. Methods Phys. Res. B* **352** 96–9
- [13] Terentyev D., Dubinko V., Bakaev A., Zayachuk Y., Van Renterghem W. and Grigorev P. 2014 *Nucl. Fusion* **54** 042004
- [14] Zhou H.B., Liu Y.L., Jin S., Zhang Y., Luo G.N. and Lu G.H. 2010 *Nucl. Fusion* **50** 025016
- [15] Veen A.V., Filius H.A., Vries J.D., Bijkerk K.R., Rozing G.J. and Segers D. 1988 *J. Nucl. Mater.* **155–7** 1113–7
- [16] Shu W.M., Kawasuso A. and Yamanishi T. 2009 *J. Nucl. Mater.* **386–88** 356–9
- [17] Shu W.M., Wakai E. and Yamanishi T. 2007 *Nucl. Fusion* **47** 201–9
- [18] Matsui T., Muto S. and Tanabe T. 2000 *J. Nucl. Mater.* **283** 1139–43

- [19] Shimada T., Kikuchi H., Ueda Y., Sagara A. and Nishikawa M. 2003 *J. Nucl. Mater.* **313** 204–8
- [20] Funabiki T., Shimada T., Ueda Y. and Nishikawa M. 2004 *J. Nucl. Mater.* **329** 780–4
- [21] Quastel A.D., Davis J.W., Haasz A.A. and Macaulay-Newcombe R.G. 2006 *J. Nucl. Mater.* **359** 8–16
- [22] Poon M., Haasz A.A. and Davis J.W. 2008 *J. Nucl. Mater.* **374** 390–402
- [23] Venhaus T., Causey R., Doerner R. and Abeln T. 2001 *J. Nucl. Mater.* **290–3** 505–8
- [24] Johnson D.F. and Carter E.A. 2010 *J. Mater. Res.* **25** 315–27
- [25] Castin N., Bonny G., Bakaev A., Ortiz C., Sand A. and Terentyev D. 2018 *J. Nucl. Mater.* **500** 15–25
- [26] Alimov V.K., Tyburska-Püschel B., Hatano Y., Roth J., Isobe K., Matsuyama M. and Yamanishi T. 2012 *J. Nucl. Mater.* **420** 370–3
- [27] Hatano Y., Shimada M., Otsuka T., Oya Y., Alimov V.K., Hara M., Shi J., Kobayashi M., Oda T. and Cao G. 2013 *Nucl. Fusion* **53** 073006
- [28] Zhu X.L., Zhang Y., Cheng L., Yuan Y., Temmerman G.D., Wang B.Y., Cao X.Z. and Lu G.H. 2016 *Nucl. Fusion* **56** 036010
- [29] Ogorodnikova O., Tyburska B., Alimov V.K. and Ertl K. 2011 *J. Nucl. Mater.* **415** S661–6
- [30] Chen Y.S., Haley D., Gerstl S.S., London A.J., Sweeney F., Wepf R.A., Rainforth W.M., Bagot P.A. and Moody M.P. 2017 *Science* **355** 1196–9
- [31] Cairney J. 2017 *Science* **355** 1128–9
- [32] Lu G.-H., Zhou H.-B. and Becquart C.S. 2014 *Nucl. Fusion* **54** 086001
- [33] Fernandez N., Ferro Y. and Kato D. 2015 *Acta Mater.* **94** 307–18
- [34] Ohsawa K., Eguchi K., Watanabe H., Yamaguchi M. and Yagi M. 2012 *Phys. Rev. B* **85** 094102
- [35] Zhou H.-B., Liu Y.-L., Jin S., Zhang Y., Luo G.-N. and Lu G.-H. 2010 *Nucl. Fusion* **50** 115010
- [36] Ren F., Yin W., Yu Q., Jia X., Zhao Z. and Wang B. 2017 *J. Nucl. Mater.* **491** 206–12
- [37] Heinola K., Ahlgren T., Nordlund K. and Keinonen J. 2010 *Phys. Rev. B* **82** 094102
- [38] You Y.-W., Li D., Kong X.-S., Wu X., Liu C., Fang Q., Pan B., Chen J. and Luo G.-N. 2014 *Nucl. Fusion* **54** 103007
- [39] Sun L., Jin S., Li X.C., Zhang Y. and Lu G.H. 2013 *J. Nucl. Mater.* **434** 395–401
- [40] Middleburgh S.C., Voskoboinikov R.E., Guenette M.C. and Riley D.P. 2014 *J. Nucl. Mater.* **448** 270–5
- [41] Oda T., Zhu D. and Watanabe Y. 2015 *J. Nucl. Mater.* **467** 439–47
- [42] Wang L.F., Shu X., Lu G.H. and Gao F. 2017 *J. Phys.: Condens. Matter* **29** 435401
- [43] Li X.-C., Gao F. and Lu G.-H. 2009 *Nucl. Instrum. Methods Phys. Res. B* **267** 3197–9
- [44] Fu B., Qiu M., Cui J., Li M. and Hou Q. 2018 *J. Nucl. Mater.* **508** 278–85
- [45] Meng C., Hao J., Xu K., Wang L.-F., Shu X., Jin S. and Lu G.-H. 2019 *Sci. China Phys. Mech.* **62** 17111
- [46] Oda T., Shimada M., Zhang K., Calderoni P., Oya Y., Sokolov M., Kolasinski R., Sharpe J.P. and Hatano Y. 2011 *Fusion Sci. Technol.* **60** 1455–8
- [47] Becquart C.S., Domain C., Sarkar U., Debacker A. and Hou M. 2010 *J. Nucl. Mater.* **403** 75–88
- [48] Wirth B.D., Hammond K., Krashennnikov S. and Maroudas D. 2015 *J. Nucl. Mater.* **463** 30–8
- [49] Kresse G. and Furthmüller J. 1996 *Phys. Rev. B* **54** 11169–86
- [50] Kresse G. and Hafner J. 1993 *Phys. Rev. B* **47** 558–61
- [51] Perdew J.P. and Wang Y. 1992 *Phys. Rev. B* **45** 13244
- [52] Monkhorst H.J. and Pack J.D. 1976 *Phys. Rev. B* **13** 5188
- [53] Ma F.-F., Wang W., Li Y.-H., Zhou H.-B. and Lu G.-H. 2018 *Nucl. Fusion* **58** 096026
- [54] Lany S. and Zunger A. 2008 *Phys. Rev. B* **78** 235104
- [55] Lany S. and Zunger A. 2009 *Modelling Simul. Mater. Sci. Eng.* **17** 084002
- [56] Freysoldt C., Neugebauer J. and Van de Walle C.G. 2009 *Phys. Rev. Lett.* **102** 016402
- [57] Lee S.C., Choi J.H. and Lee J.G. 2009 *J. Nucl. Mater.* **383** 244–6
- [58] You Y.W., Kong X.S., Wu X.B., Xu Y.C., Fang Q.F., Chen J.L., Luo G.N., Liu C.S., Pan B.C. and Wang Z. 2013 *AIP Adv.* **3** 012118
- [59] Hayward E. and Fu C.-C. 2013 *Phys. Rev. B* **87** 174103
- [60] You Y.-W., Kong X.-S., Wu X.-B., Fang Q., Chen J.-L., Luo G.-N. and Liu C. 2013 *J. Nucl. Mater.* **433** 167–73
- [61] Huang G.-Y., Juslin N. and Wirth B.D. 2016 *Comput. Mater. Sci.* **123** 121–30
- [62] Heinola K., Djurabekova F. and Ahlgren T. 2017 *Nucl. Fusion* **58** 026004
- [63] Masuda K. 1982 *J. Phys.* **43** 921–30
- [64] Muzyk M., Nguyen-Manh D., Kurzydowski K., Baluc N. and Dudarev S. 2011 *Phys. Rev. B* **84** 104115
- [65] Sun C.Q. 2007 *Prog. Solid State Chem.* **35** 1–59
- [66] Lu G.-H., Deng S., Wang T., Kohyama M. and Yamamoto R. 2004 *Phys. Rev. B* **69** 134106
- [67] Hu Y.J., Fellingner M.R., Bulter B.G., Wang Y., Darling K.A., Kecskes L.J., Trinkle D.R. and Liu Z.K. 2017 *Acta Mater.* **141** 304–16
- [68] Dezerald L., Ventelon L., Clouet E., Denoual C., Rodney D. and Willaime F. 2014 *Phys. Rev. B* **89** 024104
- [69] Ahlgren T., Heinola K., Vörtler K. and Keinonen J. 2012 *J. Nucl. Mater.* **427** 152–61
- [70] Roszell J., Haasz A. and Davis J. 2011 *J. Nucl. Mater.* **415** S641–4
- [71] Bakaev A., Grigorev P., Terentyev D., Bakaeva A., Zhurkin E. and Matrikov Y.A. 2017 *Nucl. Fusion* **57** 126040
- [72] Yajima M., Yoshida N., Kajita S., Tokitani M., Baba T. and Ohno N. 2014 *J. Nucl. Mater.* **449** 9–14
- [73] Zibrov M., Ryabtsev S., Gasparyan Y. and Pisarev A. 2016 *J. Nucl. Mater.* **477** 292–7
- [74] Ryabtsev S., Gasparyan Y., Zibrov M., Shubina A. and Pisarev A. 2016 *Nucl. Instrum. Methods Phys. Res. B* **382** 101–4
- [75] Lee H., Haasz A., Davis J., Macaulay-Newcombe R., Whyte D. and Wright G. 2007 *J. Nucl. Mater.* **363** 898–903
- [76] Shu W.M., Nakamichi M., Alimov V.K., Luo G.N., Isobe K. and Yamanishi T. 2009 *J. Nucl. Mater.* **390** 1017–21
- [77] Mundy J., Rothman S., Lam N., Hoff H. and Nowicki L. 1978 *Phys. Rev. B* **18** 6566
- [78] Ahlgren T., Heinola K., Juslin N. and Kuronen A. 2010 *J. Appl. Phys.* **107** 033516
- [79] Tyburska B., Alimov V.K., Ogorodnikova O.V., Schmid K. and Ertl K. 2009 *J. Nucl. Mater.* **395** 150–5
- [80] Alimov V.K., Tyburska-Püschel B., Lindig S., Hatano Y., Balden M., Roth J., Isobe K., Matsuyama M. and Yamanishi T. 2012 *J. Nucl. Mater.* **420** 519–24
- [81] Založnik A., Markelj S., Schwarz-Selinger T. and Schmid K. 2017 *J. Nucl. Mater.* **496** 1–8